The Role of the Droplet Interface in Controlling the Multiphase Oxidation of Thiosulfate by Ozone

Alexandra M. Deal[1], Franky Bernal[1,2], Andreas Siebert[1,3], Alexander M. Prophet[1,2], Mauricio Lopez Luna[1], Monika Blum[1,3], Richard J. Saykally[1,2], and Kevin R. Wilson[1,*]

[1]Chemical Sciences Division, Lawrence Berkeley National Laboratory, Berkeley, CA 94720, United States
[2]Department of Chemistry, University of California, Berkeley, Berkeley, CA 94720, United States
[3]Advanced Light Source, Lawrence Berkeley National Laboratory, Berkeley, CA 94720, United States
*Corresponding Author; krwilson@lbl.gov

Abstract

Predicting reaction kinetics in aqueous microdroplets, including aerosols and cloud droplets, is challenging due to the probability that the underlying reaction mechanism can occur both at the surface and in the interior of the droplet. Here, we use a stochastic reaction-diffusion model of thiosulfate oxidation by gas phase ozone to examine how the interface influences the multiphase
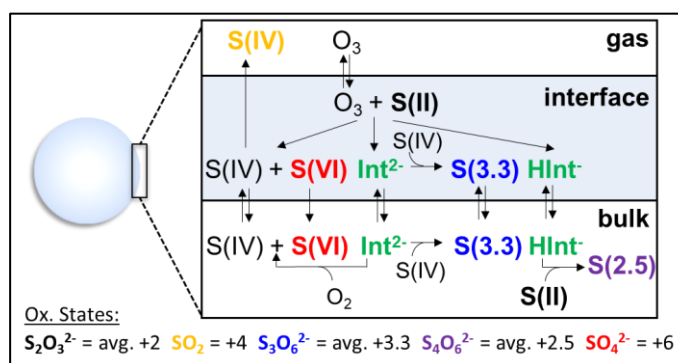
reaction kinetics measured in levitated microdroplets using mass spectrometry. Building a realistic kinetic model of multiphase reactions requires both a detailed multistep reaction mechanism as well as the surface affinities of all reactants and products. Deep-UV Second Harmonic Generation spectroscopy is used to probe surface affinities of thiosulfate, sulfate, and sulfite, key species in the reaction mechanism. Thiosulfate has an appreciable surface affinity with a measured Gibbs free energy of adsorption of -7.29 ± 2.47 kJ/mol in neutral solution, while sulfate and sulfite exhibit negligible surface propensity. The Gibbs free energy is combined with data from liquid flat jet ambient pressure x-ray photoelectron spectroscopy to constrain the concentration of thiosulfate at the surface in the kinetic model. Kinetic simulations show that the primary reaction between thiosulfate and ozone occurs at the interface and in the bulk, with the contribution of the interface decreasing from ~65% at pH 5 to ~45% at pH 13. Additionally, sulfate, the major product of thiosulfate ozonation and an important species in atmospheric processes, can be produced by two different pathways at pH 5, one with a contribution from the interface of >70% and the other occurring predominantly in the bulk (>98%). Finally, we use the kinetic model to demonstrate the impact of a range of atmospherically relevant droplet sizes and reactant concentrations on product distributions and relative importances of surface and bulk chemistry. The observations in this work have implications for mining wastewater remediation and are likely applicable to other atmospherically-relevant reaction mechanisms, suggesting that future microdroplet/aerosol chemistry studies should carefully consider the role of both interfacial and bulk chemistry.

1. Introduction

Chemistry in microdroplets has garnered interest in recent years for its (sometimes extreme) differences from either purely gas-phase or condensed phase chemistry.[1] Some studies have shown that microdroplet reaction rates increase with decreasing droplet size and reactant concentration, attributing this rate enhancement to high surface-to-volume ratios and increased contributions to the reaction from droplet interfaces. However, there is debate regarding the source of reaction rate enhancement,[2-4] and determining the exact drivers in microdroplet chemistry, including the individual contributions from surface and bulk phases, is notoriously challenging due to experimental constraints and a lack of available surface activity data. Chemistry in microdroplets, including aerosols and cloud droplets, has a crucial role in atmospheric chemistry,[5] hence a thorough understanding of microdroplet reaction mechanisms will be vital for accurate atmospheric chemistry modeling.

The oxidation of sulfur and its impact on global climate has long been studied, but new sulfur intermediates are still being identified[6] and sulfur oxyanions like thiosulfate may be underappreciated atmospheric intermediates. Thiosulfate might be released into the environment from incompletely treated mining tailings or formed from H_2S and SO_2 in volcanic stratospheric aerosols.[7] Once released or formed, the ozonation of thiosulfate can acidify the reaction environment and form a mixture of fully oxidized sulfur (sulfate, SO_4^{2-}) and partially oxidized sulfur (sulfur dioxide, SO_2, trithionate, $S_3O_6^{2-}$, and tetrathionate, $S_4O_6^{2-}$). While sulfate directly contributes to the global radiation budget through new particle formation, thiosulfate, SO_2, trithionate, and tetrathionate can act as long-lived metastable intermediates in the atmospheric sulfur cycle with down-stream environmental effects. Despite these potential impacts, the chemistry of thiosulfate in microdroplets has largely been unaccounted for in modeling the atmospheric sulfur cycle, and few studies have directly addressed the aqueous surface activity of sulfur oxyanions.

2

Efforts towards understanding the ozone oxidation of thiosulfate can also provide an excellent model system for understanding complex multistep reaction kinetics in microdroplets. Thiosulfate is often used as an O_3 scavenger in laboratory uptake studies due to its fast reaction with ozone,[8] and trapped droplet studies suggest that thiosulfate is relatively surface active.[9] In fact, previous work from Wilson and co-workers have shown that ozone reactions with organic and inorganic species in aqueous microdroplets are mediated by the non-reactive partitioning and diffusion of reactants, but many of these studies had undetectable products.[10, 11] A detailed investigation of the multiphase chemistry of thiosulfate in microdroplets can therefore add to this body of work by exploring the role of the droplet surface for a reaction where the quantitative kinetics of intermediates and products are measured.

Scheme 1. Reaction mechanism for the oxidation of aqueous thiosulfate ($S_2O_3^{2-}$) by ozone (O_3).[a]
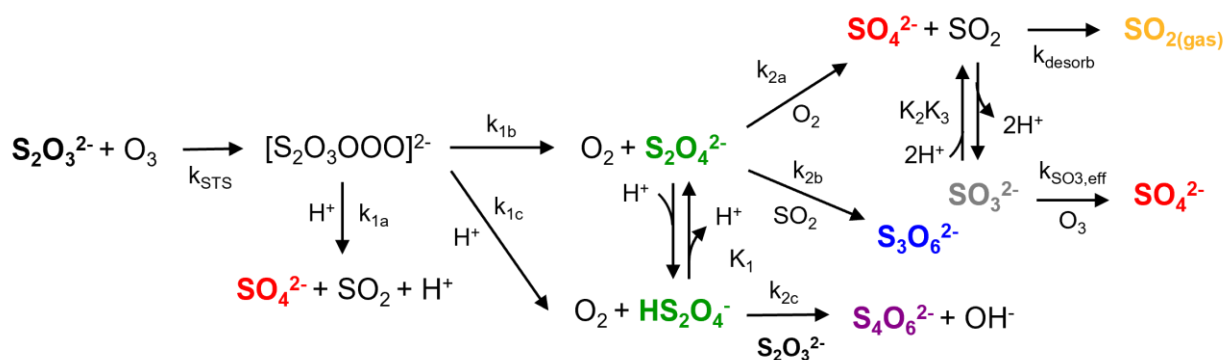
[a]Reprinted with permission from Deal, *et al.*[7] Copyright 2024 American Chemical Society.

Our previous study[7] presented the ozone oxidation of thiosulfate in aqueous droplets as a function of solution pH and gas-phase ozone concentration. This work prompted the formulation of a new reaction mechanism, shown in Scheme 1, which incorporates a previously unobserved intermediate, dithionite ($S_2O_4^{2-}$), as well as explains the pH-dependence of the reaction by a series of elementary reaction steps, as described in Deal, *et al.*[7] Briefly, the primary reaction between thiosulfate and ozone forms an ozonide intermediate ($[S_2O_3OOO]^{2-}$), which can decompose *via*

3

three different reaction steps to form sulfate (SO_4^{2-}), sulfur dioxide (SO_2), dithionite ($S_2O_4^{2-}$), and dithionite's conjugate acid ($HS_2O_4^-$). $S_2O_4^{2-}$ can then react with dissolved oxygen to form SO_4^{2-} and SO_2 or react with SO_2 to form trithionate ($S_3O_6^{2-}$). $HS_2O_4^-$ can react with another thiosulfate molecule to form tetrathionate ($S_4O_6^{2-}$). Any SO_2 produced can either desorb to the gas phase or hydrolyze to form bisulfite (HSO_3^-) and sulfite (SO_3^{2-}), which acidifies the solution. Lastly, SO_3^{2-} can be oxidized by ozone to form SO_4^{2-}. In this mechanism, the pH of the solution has an explicit role in the branching ratio of the three $[S_2O_3OOO]^{2-}$ decomposition pathways and controls the acid-base equilibria for $S_2O_4^{2-}$/ $HS_2O_4^-$ and $SO_2/HSO_3^-/SO_3^{2-}$. A kinetic model using this proposed mechanism was validated against prior literature experiments.[9, 12]

The kinetic model of the mechanism in Scheme 1 showed that accurate modeling of an experiment requires a thorough understanding of partitioning, but few studies have directly assessed the surface activity of thiosulfate or other intermediate sulfur oxyanions.[7] Here, Deep UV-Second Harmonic Generation (DUV-SHG) is used to determine the Gibbs free energy of adsorption of thiosulfate, sulfate, and sulfite, and ambient pressure x-ray photoelectron spectroscopy (APXPS) of a flat liquid micro-jet is used to determine the maximum surface concentration of thiosulfate. There is a longstanding history of using nonlinear SHG measurements to extract thermodynamic information about surface-active species.[13-15] These experiments help establish the molecular driving force for ions at the air-water interface when combined with corroborating information, typically from molecular dynamics simulations. In this work, we instead couple SHG studies with APXPS and kinetic experiments to assess the macroscopic impact of ions partitioning to interfaces during multiphase reactions. We use our kinetic models to test the Gibbs free energy of adsorption from SHG experiments and the maximum surface concentration from APXPS experiments. Thus, we bridge surface-specific (SHG and APXPS) and bulk (levitated microdroplet reactions) techniques to refine our understanding of the surface activity of thiosulfate and the mechanism for ozone oxidation of thiosulfate.

4

Finally, we use the kinetic model to explore the interaction between microscale reactors and reaction kinetics using calculated surface reaction fractions and demonstrate the potential impacts on product distributions for a range of environmentally relevant droplet sizes and reactant concentrations.

2. Methods

2.1. Deep UV Second Harmonic Generation (DUV-SHG)

2.1.1. Experimental Methods

We directly probe the equilibrium constants for sulfur oxyanions at the air-water interface using resonantly enhanced DUV-SHG spectroscopy. As a second-order nonlinear spectroscopy, DUV-SHG is a surface-specific molecular probe that, in the electric dipole approximation, generates signal from only the topmost molecular layers of the air-water interface. Since the full experimental approach is described elsewhere,[14, 16] only key details are provided here. The 800 nm output of a Ti:Sapphire amplifier (Spectra Physics, Spitfire) is directed to an optical parametric amplifier (TOPAS Prime) where the fundamental input wavelength is generated (386 – 440 nm). Solutions of $Na_2S_2O_3$ (Sigma Aldrich, Reddi-Dri 99%), Na_2SO_3 (Fisher, ≥98%), and Na_2SO_4 (Sigma Aldrich, Reddi-Dri 99%) were made using ultrapure 18.2 MΩ water (Millipore, Milli-Q). The fundamental was directed to solutions held in Petri dishes at an angle 60° relative to the solution surface normal. DUV-SHG signal from the solution interface is spectrally filtered from the colinear fundamental and detected by a photomultiplier tube (Hamamatsu, R7154PHA). Figure 1A depicts the experimental setup and SHG process.
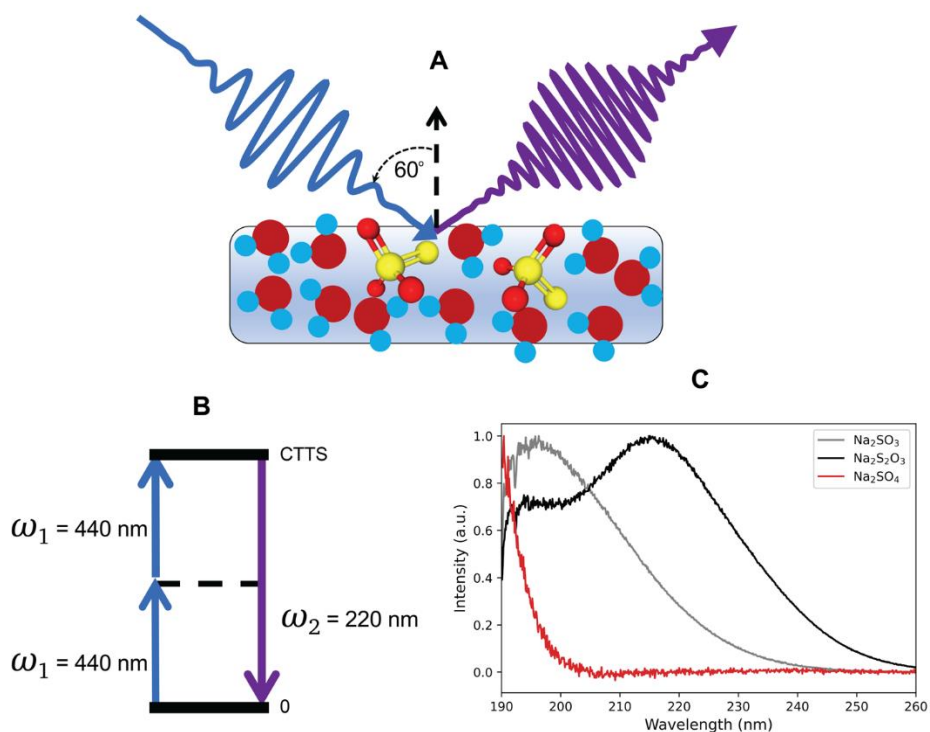
5

Figure 1. DUV-SHG experimental diagram probing thiosulfate at the air-water interface. A) Molecular depiction of SHG produced at the air-water interface containing contributions from water molecules and resonant thiosulfate anions. B) Energy-level diagram highlighting the nonlinear SHG parametric process. The fundamental at 440 nm is two-photon resonant with the CTTS transition of thiosulfate. C) UV-Visible spectra of aqueous sulfur oxyanions. The CTTS transition peaks of sulfite and thiosulfate are clearly visible along with the low energy tail of the sulfate CTTS.

In DUV-SHG, two photons are simultaneously annihilated to generate a third photon at twice the input frequency (Figure 1B). The input wavelength is chosen such that the second harmonic is resonant with the charge-transfer-to-solvent (CTTS) transition of the anions for signal enhancement. Much work has been done to characterize the energy and magnitude of CTTS transitions of common ions, including the sulfur oxyanions studied here.[17] Despite the broad absorption features typical of these transitions, the center absorption wavelengths are well separated for each of the three species studied here (Figure 1C) and therefore require different input wavelengths.

2.1.2. Langmuir Adsorption Model of DUV-SHG Spectra

To characterize the propensity of ion adsorption to the air-water interface, DUV-SHG data are fit to a Langmuir isotherm. Compared to other adsorption isotherms, a simple Langmuir model

6

best fits our concentration-dependent data. A full discussion on this Langmuir model and its application to SHG data can be found elsewhere.[14] Briefly, we assume molecules in the bulk ($[water_{(b)}]$, $[ion_{(b)}]$) are free to exchange position with molecules at the interface ($[water_{(ads)}]$, $[ion_{(ads)}]$) and derive an equilibrium expression for ion adsorption. Our model assumes that there is a maximum number of surface sites ($[sites]_{max}$) and we use the relation $[sites]_{max} = [ion_{(ads)}] + [water_{(ads)}]$ to substitute for the interfacial water concentration:

$$[water_{(ads)}] + [ion_{(b)}] \leftrightarrow [water_{(b)}] + [ion_{(ads)}] \tag{1}$$
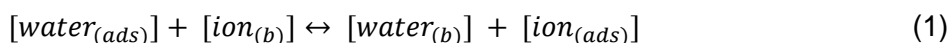
$$K_{eq}^{ads} = \frac{[water_{(b)}] \times [ion_{(ads)}]}{[water_{(ads)}] \times [ion_{(b)}]} = \frac{[water_{(b)}] \times [ion_{(ads)}]}{([sites]_{max} - [ion_{(ads)}]) \times [ion_{(b)}]} \tag{2}$$

From Equation 2, we solve for the surface ion concentration to generate Equation 3 which is in the form of a typical Langmuir expression relating ion concentration to the equilibrium constant for ion adsorption.

$$[ion_{(ads)}] = [sites]_{max} \times \frac{K_{eq}^{ads} [ion_{(b)}]}{[water_{(b)}] + K_{eq}^{ads}[ion_{(b)}]} \tag{3}$$

Being a second-order process, the measured intensity of the SHG signal ($I_{2\omega}$) is proportional to the susceptibility of the interface comprising contributions from water molecules and ions ($\chi_{water}^{(2)}, \chi_{ion}^{(2)}$), and the input intensity squared ($I_\omega{}^2$):

$$I_{2\omega} \propto \left| \chi_{water}^{(2)} + \chi_{ion}^{(2)} \right|^2 \times I_\omega{}^2 \tag{4}$$

Under resonant conditions, $\chi_{ion}^{(2)}$ is a complex quantity with both real and imaginary components. The water molecules are far from resonance and therefore $\chi_{water}^{(2)}$ has only a real contribution. Additionally, susceptibilities can be expressed as the product of the number interfacial species (N) and an average hyperpolarizability ($\langle\beta\rangle_{eff}$):

$$\frac{I_{2\omega}}{I_\omega{}^2} \propto (N_{water} \times \langle\beta\rangle_{water} + N_{ion} \times Re[\langle\beta\rangle_{ion}])^2 + (N_{ion} \times Im[\langle\beta\rangle_{ion}])^2 \tag{5}$$

Numbers of interfacial species, *N*, are converted to interfacial concentrations by dividing with N_{water}:

7

$$\frac{I_{2\omega}}{I_\omega^2} \propto \left(\langle\beta\rangle_{water} + [ion]_{surf} \times Re[\langle\beta\rangle_{ion}]\right)^2 + \left([ion]_{surf} \times Im[\langle\beta\rangle_{ion}]\right)^2 \quad (6)$$

We substitute Equation 3 into Equation 6 and group the hyperpolarizability and maximum surface site terms into **A**, **B**, and **C** parameters to generate Equation 7.

$$\frac{I_{2\omega}}{I_\omega^2} \propto \left(A + B \times \frac{K_{eq}^{ads}\,[ion_{(b)}]}{[water_{(b)}] + K_{eq}^{ads}\,[ion_{(b)}]}\right)^2 + \left(C \times \frac{K_{eq}^{ads}\,[ion_{(b)}]}{[water_{(b)}] + K_{eq}^{ads}\,[ion_{(b)}]}]\right)^2 \quad (7)$$

We can simplify Equation 7 and express all concentration terms as ion mole fractions (X_{ion}). Additionally, we multiply the fraction terms by $(K_{eq}^{ads})^{-1}/(K_{eq}^{ads})^{-1}$ and use the relation $(K_{eq}^{ads})^{-1} = e^{\frac{\Delta G}{RT}}$ to reach the final fitting equation used to relate normalized SHG intensities to Gibbs free energies of adsorption.

$$\frac{I_{2\omega}}{I_\omega^2} \propto \left(A + B\,\frac{X_{ion}}{(1-X_{ion})e^{\frac{\Delta G}{RT}} + X_{ion}}\right)^2 + \left(C\,\frac{X_{ion}}{(1-X_{ion})e^{\frac{\Delta G}{RT}} + X_{ion}}\right)^2 \quad (8)$$

2.2. Ambient Pressure Photoelectron Spectroscopy (APXPS)

We directly probe the surface concentration, $[S_2O_{3\,(ads)}^{2-}]$, of thiosulfate given its known bulk concentration, $[S_2O_{3\,(b)}^{2-}]$, using APXPS on a flat liquid jet. APXPS measurements were conducted at the Advanced Light Source (ALS) at beamline 11.0.2.1 in the LARaXS endstation using a colliding micro-liquid flat jet system, as described in Section S2.1 in the Supporting Information. O 1s core level spectra were taken with varying excitation energies (Section S2.2 in Supporting Information) to probe the first ~1.5 – 5 nm of the flat jet surface. Thiosulfate and water peak areas were determined from the O 1s spectrum, which probes the first ~1.5 nm of the surface (*i.e.,* the O 1s spectrum taken with an excitation energy producing electrons with 100 eV excess kinetic energy). These areas were used to calculate the concentration of adsorbed thiosulfate at a bulk concentration of 0.5 M, $[S_2O_{3\,(ads)}^{2-}]^{b=0.5\,M} = 0.4 \pm 0.2\,M$ (Section S2.3 in Supporting Information). The average value for $[S_2O_{3\,(ads)}^{2-}]^{b=0.5\,M}$ (0.4 M), the average plus one standard deviation (0.6 M), and the average minus one standard deviation (0.4 M) were then used with the average value for the Gibbs free energy of absorption from the DUV-SHG experiments (-7.29 kJ/mol, Figure 2B) to

8

calculate a range for the maximum concentration of adsorbed thiosulfate, which is equal to [sites]$_{max}$ in Equation 3 (see Supporting Information Section S3 for more details). This resulted in $\left[S_2O_{3\,(ads)}^{2-}\right]_{max} = 1.67 \pm 1.34\ M$.

2.3. Kinetic Modeling of Thiosulfate Ozonation

A stochastic reaction diffusion model is implemented in Kinetiscope©, which has been used to model kinetics in a variety of systems, including organic aerosol, aqueous microdroplets, and emulsions.[10, 11, 18, 19] The model used in this work was developed previously in Deal, *et al.*[7] and validated against experimental data, which is replicated here in Figure 3 and Figure 4. These data[7] were collected using levitated microdroplets that were trapped using a quadrupole electrodynamic trap (QET), exposed to ozone, and ejected into an open-port sampling interface (OPSI) for analysis by mass spectrometry (see Figure S12 in Supporting Information for an experimental schematic). The droplets comprised a 0.25 M solution of sodium thiosulfate at pH 5, 9, or 13. Solutions at pH 5 and 9 were buffered using malonic acid and NaOH or glycine and HCl, respectively. The pH 13 solution was adjusted using NaOH and was unbuffered due to a lack of viable buffers in this pH range. Single droplets were ejected sequentially and their contents at each time point were analyzed using OPSI-MS as described in Deal, *et al.*[7], providing concentrations of reactants, intermediates, and products over time. A kinetic model was constructed based on the mechanism shown in Scheme 1, with reaction rate constants and diffusion coefficients from the literature or benchmarked against the experimental data (see Table S1 in Supporting Information). This kinetic model is the basis for many of the observations in this paper and we thus describe the model in more detail here.

Kinetiscope© is a kinetic modeling software package that uses a Monte Carlo approach to simulate chemical kinetics wherein probabilities for each reaction step are used to propagate concentrations in time. To account for the multiphase nature of the droplet, the system is modeled as two rectangular compartments: a surface compartment and a bulk compartment. The surface

9

compartment has a depth of 1 nm, representing the depth of favorable solvation of ozone as determined by molecular dynamics simulations,[10] and the bulk compartment has a length of r/3, which preserves the correct surface-to-volume ratio of spherical droplets.[20] Both surface and bulk compartments have cross sections of 1 nm^2. We note that the probing depth of the DUV-SHG is a few molecules and APXPS is the first ~1.5 nm of the surface, but we model the depth of the interface as 1 nm to represent the region where ozone is expected to have enhanced concentration relative to the gas and bulk phases (see Supporting Information Figure S13). Using a larger depth for the surface compartment would over predict the amount of adsorbed ozone and inaccurately enhance thiosulfate decay.

When modeling 'bulk-only' chemistry and calculating surface reaction fractions, we add a third 'reaction-diffusion' compartment between the surface and bulk compartments, as described in Section S1.2 in Supporting Information. While this three-compartment model provides more detailed simulations, it is also computationally expensive and takes up to 24 hours to simulate ~500 seconds of reaction time, while the two-compartment model takes 15 minutes to simulate ~1,500 seconds of reaction time. Given that the two-compartment model adequately replicates the kinetics simulated in three-compartments (see Section S1.3 in Supporting Information), the two-compartment is used for all simulations unless noted otherwise.

2.3.1. Ozone Partitioning Scheme

In the model it is necessary to consider ozone in three separate regimes: gas, bulk, and at the interface.[11] For the interface, we use a previously published Langmuir adsorption framework[21] wherein ozone adsorbs to a surface site from the gas or liquid phase via the equilibria shown as steps S1 and S2 in Table S1 in Supporting Information. A 'surface site' is a portion of the interface where an ozone molecule can adsorb, and the maximum concentration of surface sites in volumetric units is related to the surface excess by

$$[sites_{O_3}]_{max} = \frac{\Gamma_{O_3}^{\infty}}{\delta} \; molec \cdot cm^{-3},\tag{9}$$

10

where $\Gamma_{O_3}^{\infty}$ is the maximum 2D surface concentration and δ is the thickness of the interface being simulated. To calculate $\Gamma_{O_3}^{\infty}$, we use the inverse of the molecular area of ozone calculated by Vieceli, et al.[22] (18.5 Å²). Note that although sites are not molecules, we use the units $molec \cdot cm^{-3}$ for consistency with kinetic rates.

To determine the relevant kinetic rates, we first decompose the dimensionless Henry's law constant, H_{cc}^{gb}, into the gas-to-surface (gs) and surface-to-bulk (sb) components, $H_{cc}^{gb} = H_{cc}^{gs} \cdot H_{cc}^{sb}$, as originally shown in Willis and Wilson[11]. Molecular Dynamics (MD) simulations published by Prophet, et al.[10] provided solvation free energies, which were used to calculate the Henry's Law components, giving $H_{cc}^{gs} = 4.97$, $H_{cc}^{sb} = 0.0292$, and $H_{cc}^{gb} = 0.1451$. Note that here we use $H_{cc}^{gs} = 4.97$, which is obtained by averaging the solvation free energy across the interfacial region, while Prophet, et al.[10] used $H_{cc}^{gs} = 9.3$, which is computed from the maximum solvation free energy in the interfacial region. The simulation is not sensitive to this difference, but we believe that $H_{cc}^{gs} = 4.97$ is a more realistic representation of O₃ in the interfacial regime. Both Prophet, et al.[10] and this work use $H_{cc}^{gb} = 0.1451$, which is consistent with previous studies on ozone solvation in 1M sodium chloride solutions.[23, 24]

The Henry's Law equilibrium constants are related to kinetic parameters to describe partitioning between the phases (adsorption/desorption between the gas-phase and interface and solvation/desolvation between the interface and bulk liquid):[11]

$$H_{cc}^{gs} = \frac{[O_{3(ads)}]}{[O_{3(g)}]} = \frac{k_{ads} \cdot \Gamma_{O_3}^{\infty} \cdot \sigma}{k_{des} \cdot \delta} \tag{10}$$

$$H_{cc}^{sb} = \frac{[O_{3(b)}]}{[O_{3(ads)}]} = \frac{k_{solv} \cdot \delta}{k_{desolv} \cdot \Gamma_{O_3}^{\infty}} \tag{11}$$

Here the subscript (ads) signifies ozone adsorbed to the interface, (b) signifies bulk solvated ozone, and (g) signifies gas-phase ozone. We set the sticking coefficient, σ, to 1 for simplicity and consistency with the previous study on ozone oxidation of iodide in aqueous microdroplets.[10] The coefficients for desorption from the interface to the gas-phase ($k_{des} = 1.93 \, x \, 10^{10} s^{-1}$) and

11

solvation from the interface into the bulk liquid ($k_{solv} = 1.90 \, x \, 10^8 s^{-1}$) were obtained from prior MD simulations.[10] Rearranging Equations 10 and 11, we compute k_{ads} and k_{desolv}:

$$k_{ads} = \frac{H_{cc}^{gs} \cdot k_{des} \cdot \delta}{\Gamma_{O_3}^{\infty} \cdot \sigma} \tag{12}$$

$$k_{desolv} = \frac{k_{solv} \cdot \delta}{H_{cc}^{sb} \cdot \Gamma_{O_3}^{\infty}} \tag{13}$$

This results in rates of adsorption to the interface from the gas-phase of $k_{ads} = 1.77 \, x \, 10^{-11} cm^3 \cdot molec^{-1} \cdot s^{-1}$ and from the bulk liquid to the interface of $k_{desolv} = 1.2 \, x \, 10^{-12} cm^3 \cdot molec^{-1} \cdot s^{-1}$. These fast rates, in a stochastic simulation, often result in a rapid 'shuttling' of ozone back and forth between the gas-phase and interface, significantly lengthening simulation times. Thus, most simulations were run with 100X slower rates; i.e., $k_{ads} = 1.77 \, x \, 10^{-13} cm^3 \cdot molec^{-1} \cdot s^{-1}$ and $k_{des} = 1.93 \, x \, 10^8 s^{-1}$. In both cases, ozone transfer happens much faster than the reaction and using the slower adsorption and desorption rate constants does not affect the overall reaction kinetics while dramatically decreasing computational time.

2.3.2. Aqueous Solute Partitioning Scheme

After diffusing into the surface compartment, solutes can adsorb to the interface using a Langmuir framework, wherein the adsorption rate is proportional to the bulk concentration and the concentration of available surface sites. Using thiosulfate as an example, surface-adsorbed species at equilibrium are expressed as,

$$[S_2O_{3(ads)}^{2-}] = [S_2O_{3\,(ads)}^{2-}]_{max} \cdot \frac{K_{eq}^{ads} \cdot [S_2O_{3(b)}^{2-}]}{[water_{(b)}] + K_{eq}^{ads} \cdot [S_2O_{3(b)}^{2-}]}, \tag{14}$$

where $[water_{(b)}] = 55.5 \; M$ and

$$K_{eq}^{ads} = k_{desolv}/k_{solv}. \tag{15}$$

Note that the number of sites available is different for volatile solutes (O_3 and SO_2) and non-volatile solutes ($S_2O_3{}^{2-}$ and all other reaction intermediates and products). To our knowledge, the equilibrium constant for adsorption, K_{eq}^{ads}, and maximum surface concentration, $[S_2O_{3\,(ads)}^{2-}]_{max}$, for thiosulfate has not been measured, so we combine data obtained from DUV-SHG (Section 2.1

12

above) and APXPS (Section 2.2 above and Section S2 in Supporting Information) to constrain the maximum concentration of adsorbed thiosulfate in the kinetic experiments, $\left[S_2O_{3\,(ads)}^{2-}\right]_{max}$ (see Section S3 in Supporting Information).

The surface affinities for other non-volatile intermediates and products are also not well known. Therefore, we adopt a relative surface activity framework wherein the Langmuir equilibrium coefficient for each species is set relative to that of thiosulfate. At least one molecular dynamics study showed that sulfate is repelled from the interface,[25] and DUV-SHG results shown in Figure 2 suggest sulfite would be similarly repelled from the interface. Thus, the Langmuir equilibrium coefficients for sulfate and sulfite are set as one order of magnitude smaller than that for thiosulfate. On the other hand, other species are likely to be at least as surface active as thiosulfate, thus we set the Langmuir equilibrium coefficients for $HS_2O_4^-$, $S_3O_6^{2-}$, and $S_4O_6^{2-}$ equal to that of thiosulfate. The remaining species, $S_2O_4^{2-}$, is assigned a Langmuir equilibrium coefficient one order of magnitude larger than that of thiosulfate, which provided the best match between simulations and experiments.[7] The reverse rate constants, k_{solv}, are set to 1 x 10^3 s^{-1} for all adsorbing species, as in Prophet, *et al.*[10] This value is large enough such that the simulated kinetics are not sensitive to changes in the magnitude of k_{solv}, but small enough to prevent excessive computation time. The forward rate constants, k_{desolv}, are calculated using Equation 15.

3. Results & Discussion

3.1. Sulfur Oxyanion Surface Activities

3.1.1. DUV-SHG of Sulfite, Sulfate, and Thiosulfate

We adopt a Langmuir-Hinshelwood mechanism in the kinetic model, wherein molecules must first adsorb to the interface before they can react in the surface compartment. The concentration of adsorbed molecules is dictated by the molecule's surface activity, determined by the maximum

13

surface concentration and free energy of adsorption to the interface (ΔG_{ads}) or associated equilibrium constant for surface adsorption (K_{eq}^{ads}). See Methods section 2.3.2. for more information. However, to the best of our knowledge, few studies have measured either ΔG_{ads} or K_{eq}^{ads} for thiosulfate and the other sulfur oxyanions involved in the reaction mechanism shown in Scheme 1. Here, we use Deep UV Second Harmonic Generation (DUV-SHG) to quantitatively determine the adsorption energy for thiosulfate at pH 6 and pH 13 and qualitatively determine sulfate and sulfite adsorption at pH 6.
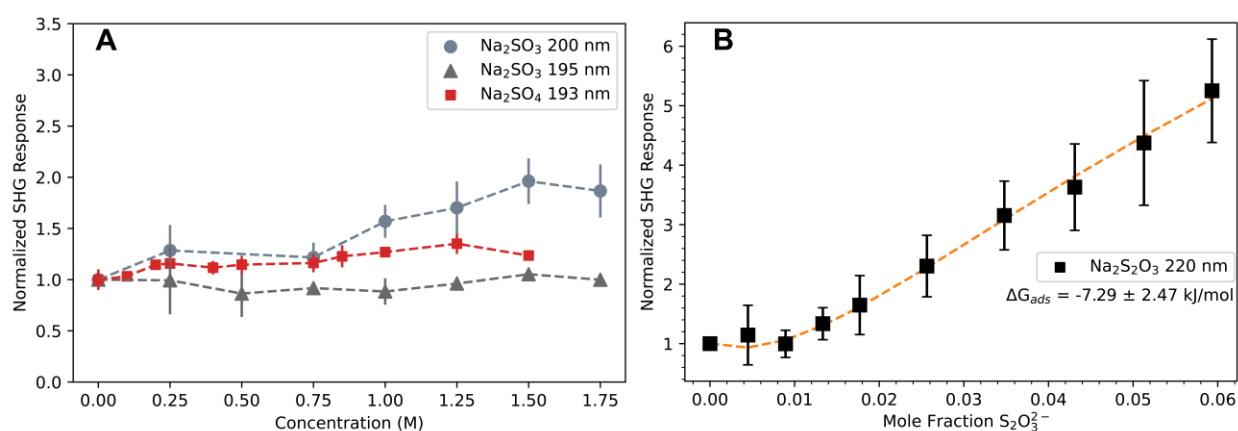
Figure 2. Normalized DUV-SHG response of sulfur oxyanions at the air-water interface. A) Response of sodium sulfite and sodium sulfate solutions exhibiting a weak concentration-dependent SHG response. Dashed lines act as a visual guide. B) Response of sodium thiosulfate exhibiting a clear concentration dependent DUV-SHG signal. Orange dashed line represents the fit to a Langmuir model. Error bars represent one standard deviation. Note that y-axes are different for clarity, panel A is shown with concentration on the x-axis for ease of interpretation, and panel B is shown with mole fraction on the x-axis for consistency with the Langmuir fit (Equation 8).

Figure 2A plots the normalized SHG response of sulfite and sulfate as a function of bulk concentration. Sulfate solutions exhibit a flat SHG response across the measured concentration range, which is consistent with sulfate being repelled from the interface. As part of the Hoffmeister series, sulfate is a known kosmotrope and several studies have found it is well-solvated in water with no significant interfacial presence.[26-29] Previous Raman thermometry measurements on 3 M aqueous $(NH_4)_2SO_4$ microdroplets observed no change in the evaporation rate relative to pure water, which suggests that neither ammonium nor sulfate significantly impacted the exchange of

14

water molecules across the air-water interface.[26] Additionally, recent phase-sensitive vibrational-SHG measurements observed minimal perturbation of the free O-H stretch band of interfacial water molecules in $MgSO_4$ and Na_2SO_4 solutions.[27] It should be noted that our sulfate measurements were made with the second harmonic ca. 20 nm away from the expected CTTS transition maximum due to limitations in our optics and to avoid water molecule transitions. However, we are still weakly resonant with the low energy tail of the CTTS as seen in Figure 1C, SHG is sensitive enough to capture signal changes even under non-resonant conditions, and our results agree with previous studies.[30]

Sodium sulfite measurements collected at 200 nm display a weak signal increase above 1 M (Figure 2A). Previous SHG work has attributed this weak linear response to an interfacial thickening of the water layer due to an increased solute concentration, which alters the hyperpolarizability of interfacial water moleucles.[16, 30, 31] Given the typical linewidth of CTTS transitions, we measured sodium sulfite at 390 nm (195 nm SHG), and observe a clear uniform response similar to sulfate measurements. If sulfite ions were indeed surface-active, a 5 nm shift away from the resonant transition center would not completely diminish the SHG response.

Unlike sodium sulfate and sodium sulfite solutions, Figure 2B shows a strong concentration dependent SHG signal for solutions of sodium thiosulfate. Fitting the normalized SHG response to Equation 8, we extract $\Delta G_{ads} = -7.29 \pm 2.47 kJ/mol$ for thiosulfate anions at the air-water interface. These results indicate that thiosulfate, a doubly charged anion, exhibits a strong propensity for the interface not seen in the similarly charged sulfite and sulfate anions. This behavior is striking since early theories of ions at interfaces by Onsager and Samaras predict a strong repulsion of doubly charged ions based on electrostatic arguments.[32] Even as early experimental and theoretical studies began to uncover support for interfacial ions, it was thought that only large, highly polarizable anions could be surface enhanced and excluded multicharged anions and cations. However, much progress has been made in our understanding of interfacial ions and we now have evidence to support the surface enhancement of previously overlooked

15

ions. Recent X-ray photoelectron spectroscopy and DUV-SHG studies find that the doubly-charged carbonate ion similarly preferentially adsorbs to the air-water interface, much more strongly than the singly charged bicarbonate ion.[31, 33] MD simulations found that carbonate ions form quasi-neutral clusters with surrounding water molecules and sodium counterions that is then better accommodated at the interface. Similarly, recent studies indicate that like-charge ion pairing is involved in the strong surface adsorption observed for guanidinium cations.[16] While we do not yet have a mechanism to explain the surface adsorption of thiosulfate, it is not unreasonable to propose that favorable ion-pairing effects are likely involved. Without MD simulations, we lack a theoretical route to validate and interpret the measured ΔG_{ads} of thiosulfate, and instead use the kinetic model to compare simulated reaction kinetics using the measured ΔG_{ads} to experimental reaction kinetics.

Specifically, Deal, *et al.*[7] performed a sensitivity analysis comparing experimental data at each pH to simulations assuming ΔG_{ads} = -4.82 kJ/mol, -7.29 kJ/mol, and -9.76 kJ/mol and found that simulations assuming ΔG_{ads} = -7.29 kJ/mol were most consistent with the pH 5 and pH 9 experimental data while simulations assuming ΔG_{ads} = -4.82 kJ/mol were most consistent with the pH 13 experimental data (see Figure S8 Supporting Information). This seems to suggest that thiosulfate is less surface-active in this highly alkaline environment, thus we perform additional DUV-SHG measurements of thiosulfate solutions adjusted to pH 13 (see Section S4 in Supporting Information). The average ΔG_{ads} value at pH 13 is more positive (-4.08 ± 2.85 kJ/mol, Figure S8 in Supporting Information) than that for the neutral solution (-7.29 ± 2.47 kJ/mol, Figure 2Figure 3B), which may be consistent with a decreased surface activity at pH 13. However, the uncertainty in these measurements remains large and the intensity of the SHG response is not significantly different than the pH 6 measurements, which is inconsistent with decreased surface activity. Thus, while our data suggest that the ΔG_{ads} of thiosulfate at the air-water interface could be less favorable with increased pH, DUV-SHG results are inconclusive on their own (see Section S4 in Supporting Information for more details).

16

3.1.2. Constraining [$S_2O_3^{2-}$(ads)] with DUV-SHG and APXPS

The concentration of adsorbed thiosulfate calculated by the kinetic model is dependent on both the free energy of adsorption, as measured by DUV-SHG and discussed previously, as well as the maximum concentration of adsorbed thiosulfate, $\left[S_2O_{3\,(ads)}^{2-}\right]_{max}$, which is determined using combined DUV-SHG and APXPS results (Section S3 in Supporting Information). To gauge the sensitivity of the coupled parameters ΔG_{ads} and $\left[S_2O_{3\,(ads)}^{2-}\right]_{max}$, we completed kinetic simulations for two scenarios, first with ΔG_{ads} = -4.82 kJ/mol and then ΔG_{ads} = -7.29 kJ/mol. For each given free energy of adsorption, three values of $\left[S_2O_{3\,(ads)}^{2-}\right]_{max}$ were tested, namely $\left[S_2O_{3\,(ads)}^{2-}\right]_{max}$ = 8.05 x10^{20} molec · cm^{-3} (1.33 M), 1.61 x10^{21} molec · cm^{-3} (2.67 M), and 2.41 x10^{21} molec · cm^{-3} (4.00 M). Experimental data recreated from Deal*, et al.*[7] (points) are compared to simulation results (lines) assuming *ΔG* = -4.82 kJ/mol in Figure 3 and simulation results assuming *ΔG* = -7.29 kJ/mol in Supporting Information Figure S7. Note that green points represent $S_2O_4^{2-}$ and $HS_2O_4^-$ and grey points represent SO_3^{2-} and HSO_3^-, as protonated forms are indistinguishable from deprotonated forms in the mass spectra used in Deal*, et al.*[7] The term 'S loss', or the total amount of reacted sulfur that is not detected in products, encompasses all potential unaccountable sulfur sinks, including evaporation as gasses, precipitation as elemental sulfur, and experimental error.[7]
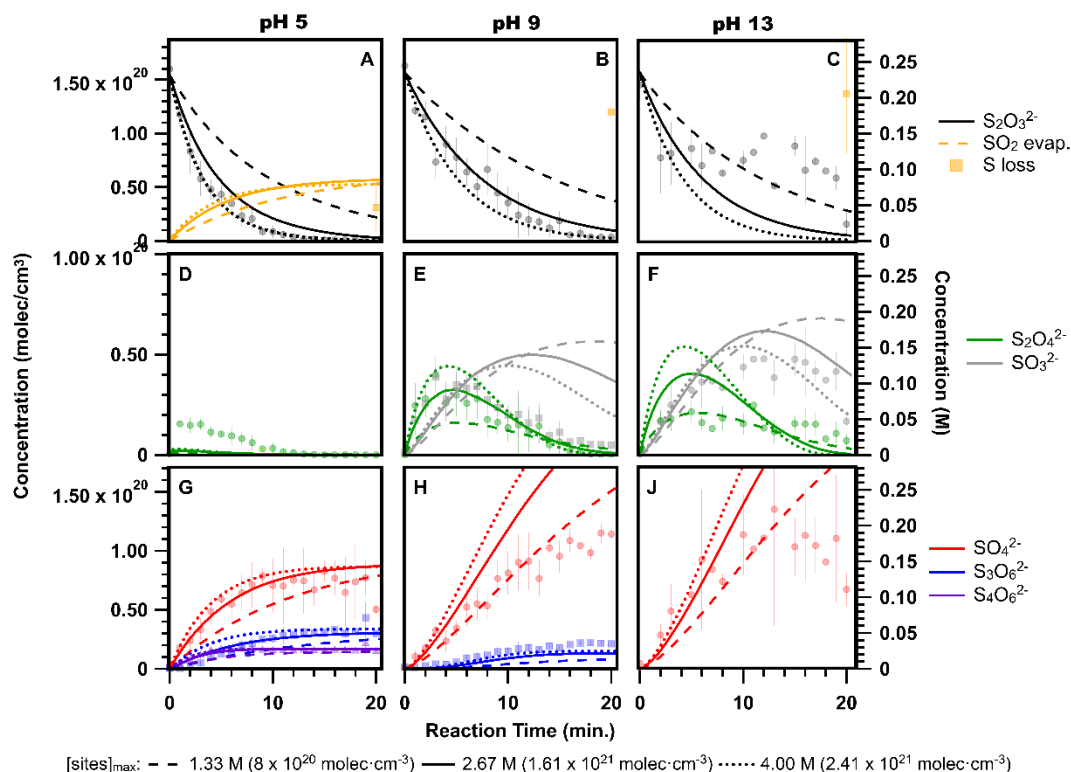
17

Figure 3. Representative reaction kinetics for the ozone oxidation of thiosulfate ($S_2O_3^{2-}$) in pH 5 (A,D,G), pH 9 (B,E,H), and pH 13 (C,F,J) solutions compared with simulation results using ΔG = -4.82 kJ/mol and three values for the maximum concentration of adsorbed thiosulfate (values shown in legend). Experimental data (points) are recreated from Deal, *et al.*[7] with error bars representing one standard deviation in a set of 5 repeats.

Interestingly, we find that the ΔG_{ads} = -4.82 kJ/mol simulations with varying $\left[S_2O_{3\ (ads)}^{2-}\right]_{max}$ recreate the experimental data at all three pH values (Figure 3), while the ΔG_{ads} = -7.29 kJ/mol simulations only recreate experimental data at pH 5 and pH 9 (Figure S7 in Supporting Information). In Figure 3, we see that $\left[S_2O_{3\ (ads)}^{2-}\right]_{max}$ = 4.00 M (dotted lines) most closely recreates the pH 5 experimental data, $\left[S_2O_{3\ (ads)}^{2-}\right]_{max}$ = 2.67 M (solid lines) most closely recreates the pH 9 experimental data, and $\left[S_2O_{3\ (ads)}^{2-}\right]_{max}$ = 1.33 M (dashed lines) most closely recreates the pH 13 experimental data. Specifically, the simulated thiosulfate decay (Figure 3A,B,C black), trithionate production (Figure 3G,H blue), and tetrathionate production (Figure 3G purple) show excellent agreement with experimental data. The simulated sulfate production (red) also shows excellent agreement with experimental data at pH 5 (Figure 3G) but overestimates

18

the amount of observed sulfate production at pH 9 (Figure 3H). This discrepancy at pH 9 is likely due to the high sulfur loss (Figure 3B orange point), which the kinetic model does not account for. Comparing the simulated and experimental results for dithionite and sulfite is more complicated due to uncertainties in the concentrations for each of these species. Dithionite is not stable in aqueous solution, where it decomposes into sulfite and sulfate,[34] meaning that calibration curves were not obtained for dithionite and the concentrations shown here are qualitative rather than quantitative. Furthermore, because dithionite decomposes into sulfite, the experimental sulfite signal at pH 9 (Figure 3E grey) may be skewed. Despite these issues, we find that the kinetic simulations do accurately replicate the kinetic behavior of dithionite (Figure 3D,E,F green).

We note that although OH$^-$ is known to react with ozone, which could also explain the reduced thiosulfate decay observed at pH 13, the rate constant (< 100 M^{-1} s^{-1} or < 2 x 10^{-19} cm^3 molec^{-1} s^{-1})[35] is ~6 orders of magnitude smaller than the rate constant for the reaction of thiosulfate with ozone (7.2 x 10^7 M^{-1} s^{-1} or 1.20 x 10^{-13} cm^3 molec^{-1} s^{-1}).[36, 37] This means that almost all of the thiosulfate has to be depleted before the OH$^-$ + O$_3$ reaction becomes competitive. Given that we still detect significant amounts of thiosulfate at long reaction times, we consider OH$^-$ + O$_3$ as a negligible contributor to the reaction kinetics. We also note that although we model the pH as the same in the bulk and surface compartments, there is some evidence for enhanced acidity near the interface.[1] While it is possible our modeling of pH is too simplistic, enhanced acidity at the interface likely does not explain the pH 13 kinetics as we would expect to see formation of trithionate or tetrathionate. On the other hand, there is some evidence that anion reactions with ozone are slower at the interface in highly alkaline environments.[10]

Overall, we find that the DUV-SHG and APXPS results are consistent with the experimental results from Deal*, et al.*[7], with all indicating that thiosulfate is surface active. Although there is some uncertainty in the free energy of adsorption, and whether it changes with pH, the DUV-SHG data show favorable free energies of adsorption to the interface in all cases. The APXPS results also show a significant concentration of thiosulfate at the water surface, with maximum surface

19

concentrations of 1.33 M to 4 M. Simulations with this range of potential maximum surface concentrations suggest that less thiosulfate adsorbs to the interface with increasing pH, which may indicate competitive adsorption between thiosulfate and OH⁻, especially at pH 13 when $[OH^-]$ = 0.1 M compared with $[S_2O_3^{2-}]$ = 0.25 M. We note that APXPS measurements have only been collected at neutral pH, and the exact mechanism for decreased thiosulfate surface concentration with increasing pH remains to be determined. However, the general trend is consistent with previous literature,[10] and both experimental and simulated kinetics results show a fast reaction with ozone which points towards a significant contribution from surface chemistry, regardless of the exact concentration of thiosulfate.

3.2. Interface vs. Bulk Contributions to Reaction Kinetics

To examine the relative contribution of surface and bulk reactions, we run the kinetic model allowing only surface or bulk chemistry, respectively. Given the findings in Section S.1., the kinetic models use ΔG_{ads} = -4.82 kJ/mol for all pH values, but use $\left[S_2 O_{3\,(ads)}^{2-}\right]_{max}$ = 4.00 M for pH 5, $\left[S_2 O_{3\,(ads)}^{2-}\right]_{max}$ = 2.67 M for pH 9, and $\left[S_2 O_{3\,(ads)}^{2-}\right]_{max}$ = 1.33 M for pH 13. 'Bulk only' simulations require an additional reaction-diffusion compartment between the surface and bulk compartments to account for near- surface reactions (see Supporting Information Section S1.2). In both 'surface only' and 'bulk only' simulations, acid-base equilibria are still enforced throughout the simulation volume and all species are allowed to adsorb to the interface, desorb from the interface, and diffuse throughout the surface and bulk compartments. Simulations run with only surface chemistry show significant thiosulfate decay (black dashed lines in Figure 4A,B,C), while modeling only bulk chemistry (dotted lines) predicts a slower thiosulfate decay at pH 5 and pH 9.

At all pH values studied here, neither surface chemistry nor bulk chemistry alone recreate the observed kinetics for reaction intermediates and final products (summarized in Table S3 in Supporting Information). As shown by the dashed lines Figure 4D,E,F, restricting chemistry to the surface does not accurately capture the decay kinetics for dithionite ($S_2O_4^{2-}$, green) and results in

20

negligible sulfite (SO_3^{2-}, grey) formation. Note that although experimental results cannot distinguish between $S_2O_4^{2-}$ and its conjugate acid, $HS_2O_4^-$, simulations suggest that $[S_2O_4^{2-}] \gg [HS_2O_4^-]$ at all pH values studied here. In Figure 4G,H,J, we see that restricting chemistry to the surface compartment produces a negligible amount of the expected final products in pH 9 and pH 13 solutions (Figure 4H,J), and no tetrathionate ($S_4O_6^{2-}$, purple) and too much trithionate ($S_3O_6^{2-}$, blue) in the pH 5 solution (Figure 4G). On the other hand, restricting chemistry to the bulk compartment shows reasonable agreement with dithionite ($S_2O_4^{2-}$, green) kinetics (Figure 4D,E,F) and reasonable agreement with the final concentrations of final products at pH 5 (Figure 4G) but does not accurately capture the maximum dithionite concentration at pH 9 (Figure 4E), final product kinetics at early times at pH 5 (Figure 4G), or trithionate ($S_3O_6^{2-}$, blue) production at pH 9 (Figure 4H). This suggests that the ozonation of thiosulfate in droplets formed from pH 5 and pH 9 solutions relies on *both* surface and bulk chemistry.
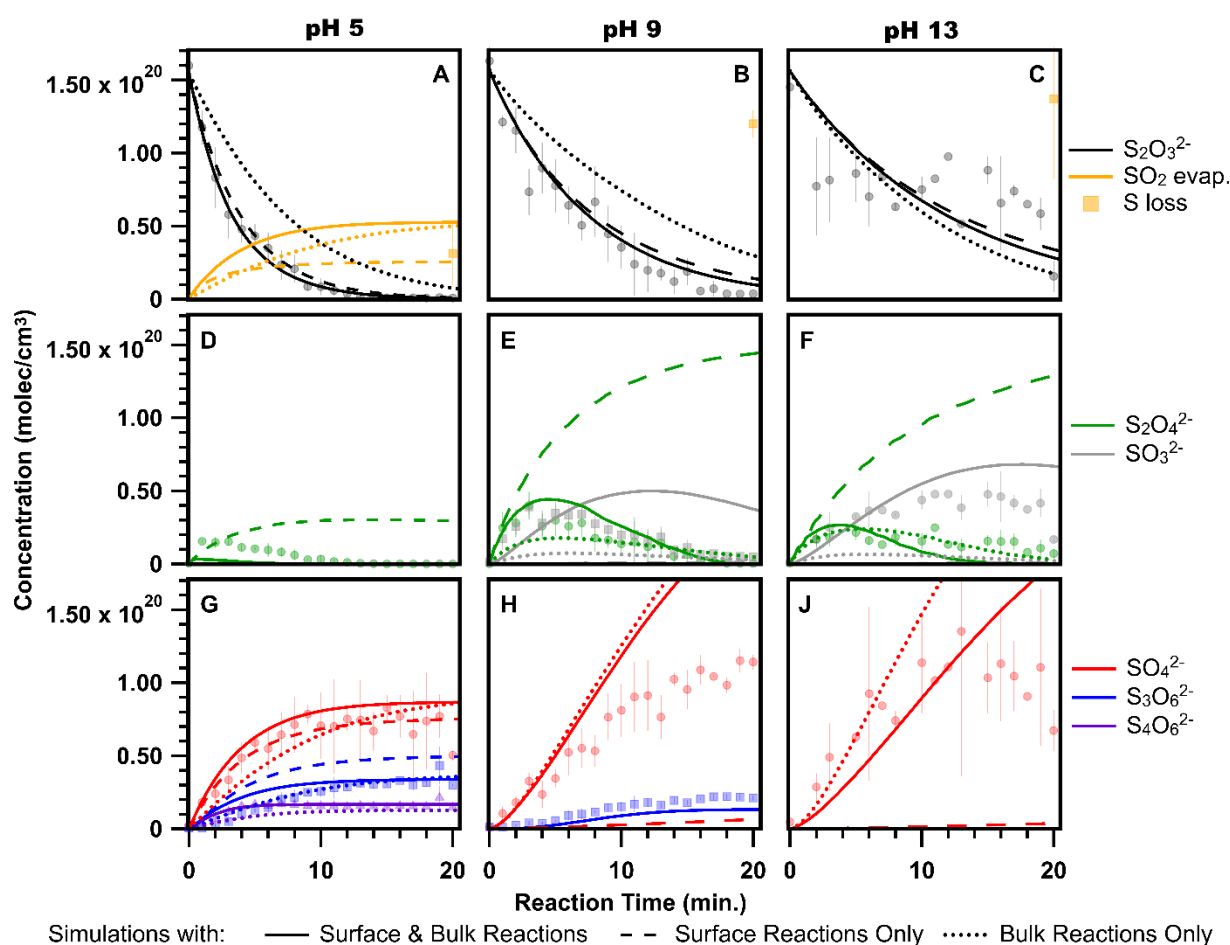
21

Figure 4. Contributions from surface and bulk chemistry to the ozone oxidation of thiosulfate ($S_2O_3^{2-}$) in pH 5 (A,D,G), pH 9 (B,E,H), and pH 13 (C,F,J) solutions. Experimental data (points) are recreated from Deal, *et al.*[7] with error bars representing the standard deviation in a set of 5 repeats. Simulation results include both surface and bulk reactions (solid lines), only surface reactions (dashed lines), or only bulk reactions (dotted lines).

Thiosulfate decay kinetics appear decoupled from the kinetics of the reaction intermediates and products, as mentioned in Deal, *et al.*[7] and seen in Figure 4. This is especially clear for pH 5 and pH 9 solutions, wherein the thiosulfate decay kinetics (Figure 4A,B) can be described using only surface reactions, but the kinetics of reaction intermediates (Figure 4D,E) and products (Figure 4G,H) must be described using both surface and bulk reactions. To better understand this, we examine the percent surface reaction for each reaction step using a 3-compartment model (see Section S1.2. and S.1.3. in Supporting Information). Although computationally expensive, a 3-compartment model is used to prevent an artificial enhancement of the surface reaction fraction,

22

and the reaction-diffusion compartment (noted as 'rxn') is considered part of the bulk. The selection frequency, n, or number of times a specific reaction step occurs, is extracted from the Kinetiscope© model for each reaction step in the bulk, reaction-diffusion, and surface compartments. The percent surface reaction, f_{surf}^x, for each reaction step, x, is then calculated as $f_{surf}^x = \frac{n_{surf}^x}{n_{surf}^x + n_{rxn}^x + n_{bulk}^x} * 100\%$. The results are shown in Figure 5.
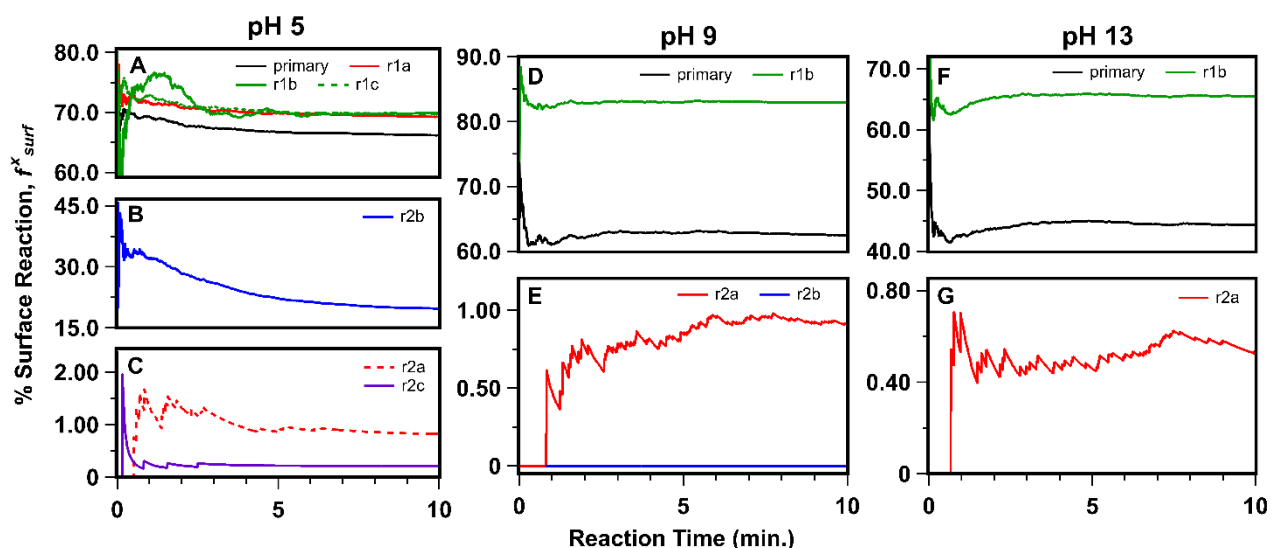
Figure 5. Percent surface reaction values for each reaction step determined from kinetic simulations. Note that y-axes vary for clarity. The colors for secondary and other down-stream reaction steps are set to match the product color scheme used elsewhere in this paper (*e.g.*, reaction 2b is set to blue to match the blue used for trithionate ($S_3O_6^{2-}$)).

Figure 5A,D,F shows that the primary reaction between thiosulfate and ozone occurs both at the surface and in the bulk at all pH values, with f_{surf}^x decreasing from over 65% at pH 5 to ~45% at pH 13, which is consistent with the decreasing value of $\left[S_2O_{3\,(ads)}^{2-}\right]_{max}$ used here. The subsequent decomposition of the ozonide intermediate $[S_2O_3OOO]^-$ to form SO_2 and sulfate, $S_2O_4^{2-}$, or $HS_2O_4^-$ (reactions 1a, 1b, 1c in Figure 5A,D,F) primarily occurs at the droplet surface at pH 9 (Figure 5D; f_{surf}^x >80%), but has a larger contribution from the bulk at pH 5 (Figure 5A; f_{surf}^x ~70%) and pH 13 (Figure 5F; f_{surf}^x ~65%). On the other hand, the oxygen-mediated

23

decomposition of $S_2O_4^{2-}$ to form SO_2 and SO_4^{2-} (reaction 2a in Figure 5C,E) and the reaction of $HS_2O_4^-$ with thiosulfate to form $S_4O_6^{2-}$ (reaction 2c in Figure 5C) occur primarily in the droplet bulk with f_{surf}^x < 2%. Interestingly, the location of the $S_2O_4^{2-}$ + SO_2 reaction to form $S_3O_6^{2-}$ (reaction 2b in Figure 5B,E) is both pH and reaction time dependent. At pH 9, this reaction occurs mostly in the droplet bulk with f_{surf}^x ~ 0% (Figure 5E), but at pH 5, this reaction occurs at the surface and in the bulk with f_{surf}^x decreasing from ~35% to ~20% over 10 minutes (Figure 5B). Using this information, we can overlay the reaction mechanism shown in Scheme 1 with the interface or bulk reaction location and create a detailed reaction-diffusion mechanism as demonstrated in Figure 6.
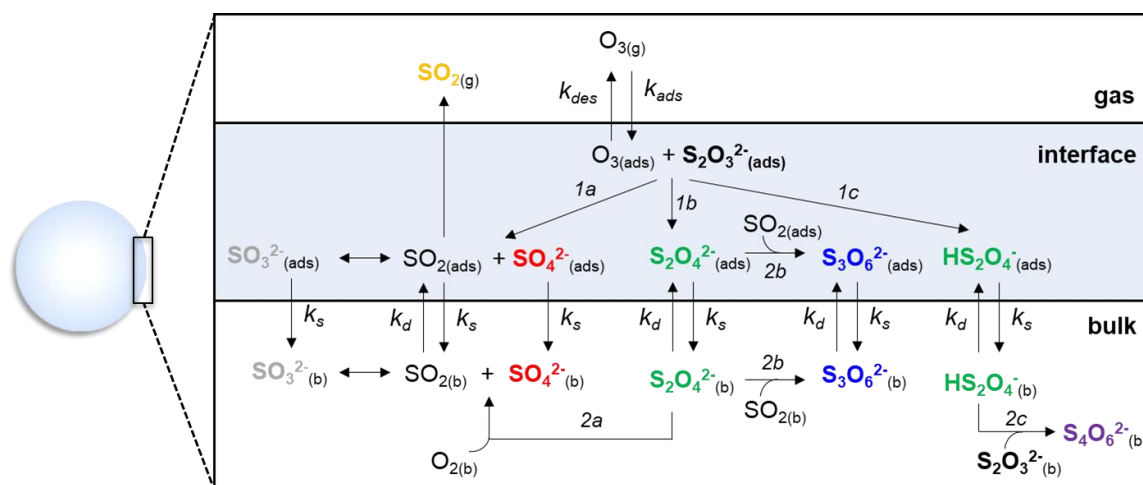

Figure 6. Schematic of the interface-mediated reaction-diffusion mechanism for the ozonation of thiosulfate in aqueous droplets at pH 5. Bolded species are detected by experiments[7] and colors are set to match those used in Scheme 1 and other figures in this work.

The combined role of pH and the interface in the production of sulfate, the main product, is particularly interesting. Sulfate can either be formed by direct decomposition of the ozonide intermediate, which primarily occurs at the interface (r1a in Figure 5A,D), or by the reaction of $S_2O_4^{2-}$ with O_2, which primarily occurs in the bulk (r2a in Figure 5C,E). However, reaction 1a is pH dependent, meaning that reaction 2a is the main sulfate formation pathway at pH 9 and pH 13. Ultimately, sulfate will be formed mostly in the bulk at higher pH, but some will be formed at the surface of the droplet at lower pH. Accurate accounting of sulfate is important for climate modeling

24

due to its hygroscopic nature and ability to form cloud condensation nuclei, meaning that such a detailed analysis of sulfate formation in droplets may be useful to atmospheric scientists.

3.3. Reactant Concentration & Droplet Size Effects

Microdroplets in the atmosphere may be exposed to a range of gas-phase reactant concentrations or have a variety of size distributions and solute concentrations. With this in mind, we seek to address how aerosol/droplet size, thiosulfate concentration, and ozone concentration affect the relative importance of the surface and bulk chemistry illustrated in Figure 6.

First, we compare our kinetic model with data published by Hsu*, et al.*[9] which utilized smaller droplets (~3 μm) and larger ranges of thiosulfate (2.86 to 10.1 M) and ozone concentrations (0.4 to 15 ppm). Hsu*, et al.*[9] used optical tweezers to capture single droplets and Raman spectroscopy to determine reactant and product concentrations. Droplets were unbuffered, and the pH likely decreased from 7 at the start of the reaction to 1 or 2 at the end of the reaction. The kinetic model used here assumes a fixed pH to reduce computation time and used pH = 7, which has been accurate when modeling other unbuffered thiosulfate ozonation experiments.[7] Despite this assumption, our model adequately predicts the thiosulfate decay detected in some of the Hsu*, et al.*[9] experiments, as shown in Figure 7. We note, however, that our model does not explain all of the Hsu*, et al.*[9] data as shown in Section S6 in Supporting Information, especially at low ozone

25

concentrations where the thiosulfate decay rate decreases and experimental error increases (Experiments 6-9 in Figure S9 and S10 in Supporting Information).
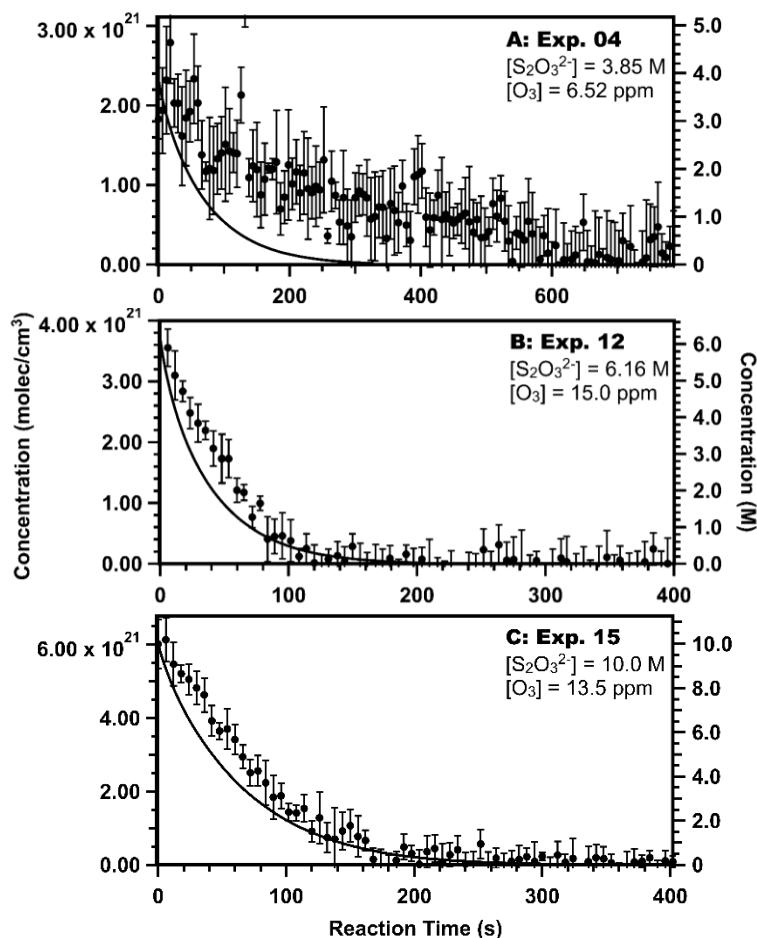

Figure 7. Select comparisons between the kinetic model (lines) and experimental data from Hsu, *et al.*[9] Data with error bars are recreated from ref [9]. See Section S6 in Supporting Information for all comparisons between model and experiments.

Next, we investigate a range of atmospherically relevant initial bulk thiosulfate concentrations, gas-phase ozone concentrations, and droplet radii using the kinetic model described here. Note that although most aerosols are very acidic (pH 1-3), our current kinetic model has not been benchmarked against experiments at such low acidity. Additionally, there are some instances where aerosols may reach pH 4-6, including over Hawaii, São Paulo, and mainland China.[38] As such, the simulations presented here use the pH 5 kinetic model to offer novel insights into the ozonation of thiosulfate in acidic environments.

26

The droplet experiments presented in Deal, *et al.*[7] were performed with an initial bulk thiosulfate concentration of 250 mM, but thiosulfate concentrations in the natural environment are likely very low (< 10 mM). Similarly, the experiments presented in Deal, *et al.*[7] were performed with gas-phase ozone concentrations between 1 and 6 ppm, but gas-phase ozone concentrations in the natural environment are much lower (< 1 ppm). Here, we connect experiment and natural environment concentration ranges by simulating droplet chemistry with $[S_2O_3^{2-}]_0$ = 1, 10, 100, and 250 mM and $[O_3]_{gas}$ = 0.1, 0.5, and 1 ppm. Atmospheric chemistry is most impacted by aerosols/droplets with radii between 0.001 and 5 μm, but at sufficiently small droplet sizes (< ~0.01 μm), curvature can affect droplet chemistry due to the similarity between molecular and droplet sizes. Given that our kinetic model does not account for droplet curvature, we simulate droplets with r = 0.2 μm (which represents a maximum in the volume distribution for a typical urban model aerosol[39]), 3 μm (representative of Hsu, *et al.*[9]), and 25 μm (representative of Deal, *et al.*[7]). Sets of simulations were run with fixed thiosulfate concentration ($[S_2O_3^{2-}]_0$ = 100 mM) or fixed ozone concentration ($[O_3]_{gas}$ = 1 ppm), and the concentrations of each product and the percent surface reactions were calculated using the values after all thiosulfate was reacted. Note that of the four products examined here, SO_4^{2-}, $S_3O_6^{2-}$, and $S_4O_6^{2-}$ were detectable in experiments and SO_2 was undetectable.[7, 9] However, SO_2 is likely a major source of the S loss noted in the Deal, *et al.*[7] experiments, Figure 3, and Figure 4, thus we model its production here. The % yield for each product represents the total amount of reacted sulfur that is incorporated into the given product, and the % surface reaction is calculated as described previously.

Figure 8 shows the impact of $[S_2O_3^{2-}]_0$, $[O_3]_{gas}$, and aerosol size on the product distribution, or % yield of each product, and relative importance of surface chemistry to bulk chemistry for a given reaction, or the % surface reaction. Note that the results in Figure 8 were calculated with the 2-compartment model described in Methods Section 2.3 to reduce computation time, and results were checked against a 3-compartment model (see Section S9 in Supporting Information). Although the 3-compartment model showed decreased % surface reaction values, the overall

27

trends with changes in $[S_2O_3^{2-}]_0$, $[O_3]_{gas}$, and r remain constant, and there were negligible differences in the calculated % yield.
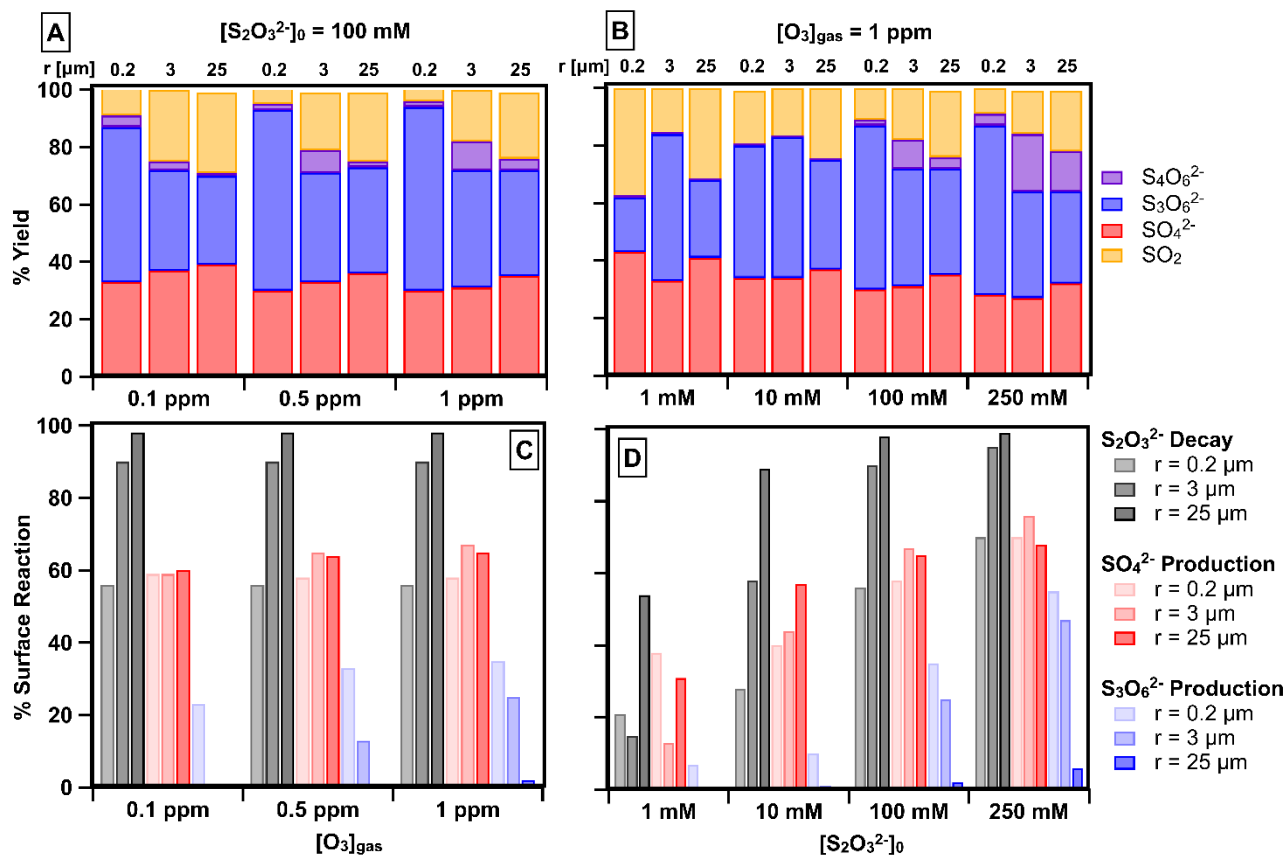

Figure 8. Product distributions (A,B) and proportion of reactions occurring at the droplet surface (C,D) for a range of gas-phase ozone concentrations ($[O_3]_{gas}$), initial bulk thiosulfate concentrations ($[S_2O_3^{2-}]_0$), and droplet radii. In A and C, the initial bulk thiosulfate concentration is fixed at 100 mM, while the gas-phase ozone concentration and droplet radius are varied. In B and D, the gas-phase ozone concentration is fixed at 1 ppm while the initial bulk thiosulfate concentration and droplet radius are varied. Note: In A and B, SO_4^{2-}, $S_3O_6^{2-}$, $S_4O_6^{2-}$, and SO_2 products are indicated by red, blue, purple, and orange, respectively, to show the % yield of each product. In C and D, $S_2O_3^{2-}$ decay, SO_4^{2-} production, and $S_3O_6^{2-}$ production are indicated by grey, red, and blue bars, respectively, with differences in shade according to droplet size as shown in the legend. Simulations presented here are run with a 2-compartment model to reduce computation time (see Methods Section 2.3. and Section S1.2. in Supporting Information). Select simulations run with a 3-compartment model are shown for comparison in Section S9 in Supporting Information.

Several observations can be drawn from Figure 8. First, changes in $[O_3]_{gas}$ have minimal impacts on the product distribution (Figure 8A) and relative importance of surface vs. bulk chemistry (Figure 8C). In contrast, $[S_2O_3^{2-}]_0$ has a significant effect on both product distributions (Figure 8B) and surface vs bulk chemistry (Figure 8D). The difference in product distributions

28

shown in Figure 8B largely stems from the competition between SO_2 evaporation (desorb in Scheme 1) and the downstream reactions that form SO_4^{2-}, $S_3O_6^{2-}$, and $S_4O_6^{2-}$ (2a, 2b, and 2c in Scheme 1 and Figure 6). Specifically, we see that as $[S_2O_3^{2-}]_0$ increases, the % yield of $S_4O_6^{2-}$ also increases because its production requires two thiosulfate molecules, while the % yield of SO_4^{2-} and SO_2 decreases. As $[S_2O_3^{2-}]_0$ increases, more thiosulfate decay, SO_4^{2-} production, and $S_3O_6^{2-}$ production occur at the surface (Figure 8D) due to the Langmuir adsorption of thiosulfate to the interface. At higher bulk concentrations, more thiosulfate will adsorb to the interface, depleting a significant portion of the adsorbed ozone before it can enter the droplet bulk. At lower thiosulfate concentrations, which will have less adsorbed thiosulfate, less surface adsorbed ozone will be reacted, allowing more ozone to enter the droplet bulk, thereby increasing the number of bulk reactions and decreasing the relative importance of surface reactions.

Finally, we examine the role of droplet size in relationship to the reacto-diffusive length, l. The reacto-diffusive length is calculated as:

$$l = \sqrt{\frac{D_{O_3}}{k \cdot [S_2O_{3(b)}^{2-}]}}, \tag{16}$$

where D_{O_3} is the diffusion coefficient for ozone and k is the rate constant for the reaction between ozone and thiosulfate (see Section S1 in Supporting Information for these values). For the bulk thiosulfate concentrations tested here (1 mM, 10 mM, 100 mM, 250 mM), we calculate reacto-diffusive lengths of approximately 150nm, 50 nm, 15 nm, and 10 nm, respectively.

For a given $[O_3]_{gas}$ and $[S_2O_3^{2-}]_0$, increasing droplet size increases the % surface reaction for $S_2O_3^{2-}$ decay and decreases the % surface reaction for $S_3O_6^{2-}$ production (gray and blue in Figure 8C,D). In larger droplets, where the radius is much larger than the reacto-diffusive length, bulk chemistry is limited by diffusion, resulting in ozonation reactions occurring mostly at the surface. In smaller droplets, the radius of the droplet nears the reacto-diffusive length, approaching phase mixing where ozone diffusion no longer limits bulk phase reactions. This also leads to differences in product distributions due to the phase dependent competition of downstream reaction steps,

29

as shown in Figure 6. Generally, for a given $[O_3]_{gas}$ and $[S_2O_3^{2-}]_0$, the % yields of SO_4^{2-} and SO_2 increase with increasing droplet size, while the relationships between droplet size and the % yields of $S_3O_6^{2-}$ or $S_4O_6^{2-}$ are more complicated (Figure 8A,B).

Droplet size and $[S_2O_3^{2-}]_0$ effects on product distributions are particularly interesting when considering the impacts on the overall oxidation state of sulfur, as shown in Figure 9. $S_2O_3^{2-}$ has an average oxidation state of 2, while the major products have a variety of oxidation states. SO_4^{2-} has an oxidation state of 6, SO_2 has an oxidation state of 4, $S_3O_6^{2-}$ has an average oxidation state of 3.3, and $S_4O_6^{2-}$ has an average oxidation state of 2.5. This means that reaction environments that favor $S_3O_6^{2-}$ and/or $S_4O_6^{2-}$ will, on average, produce less oxidized sulfur than reaction environments that favor SO_2 and/or SO_4^{2-}. Among the test environments simulated here, the smallest droplets (r = 0.2 μm) with the lowest $[S_2O_3^{2-}]_0$ (1 mM) produce the most sulfate and SO_2, resulting in the highest average oxidation state at reaction completion (4.74). This is in contrast with midsize droplets (r = 3 μm) with the highest $[S_2O_3^{2-}]_0$ (250 mM), which produce the most $S_4O_6^{2-}$, resulting in the lowest average oxidation state at reaction completion (3.99).
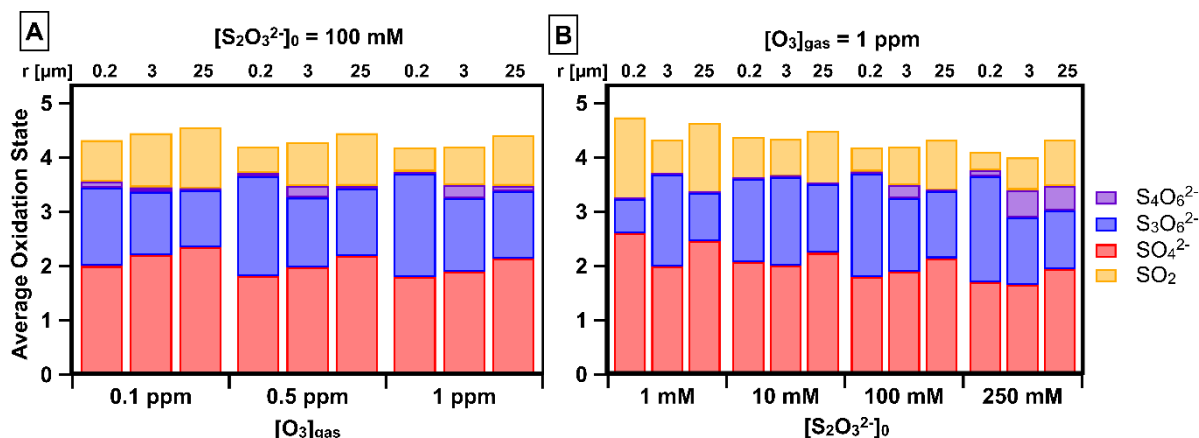

Figure 9. Average sulfur oxidation state for a range of gas-phase ozone concentrations, $[O_3]_{gas}$, (A), initial bulk thiosulfate concentrations ($[S_2O_3^{2-}]_0$), (B) and droplet radii (indicated across the top of each panel. Note: The average oxidation state is broken down into contributions from each product. Contributions from SO_4^{2-}, $S_3O_6^{2-}$, $S_4O_6^{2-}$, and SO_2 are indicated by red, blue, purple, and orange, respectively.

The average sulfur oxidation state is a function of the product distribution, which will be determined by a combination of droplet size and thiosulfate concentration, primarily due to an

30

interface-mediated competition between SO_4^{2-} and $S_4O_6^{2-}$ production. As depicted in Figure 6, $S_4O_6^{2-}$ production requires the reaction of thiosulfate with ozone, which primarily occurs at the surface, followed by the secondary reaction of $HS_2O_4^-$ with another thiosulfate molecule, which primarily occurs in the bulk. In contrast, SO_4^{2-} production occurs by two different pathways, at the interface or in bulk. Given this complex role of the droplet interface in controlling individual reaction steps, it is unsurprising that the product distribution, and thus the overall oxidation state, is a complex function of thiosulfate concentration and droplet size. Regardless of the exact mechanistic differences that drive this outcome, this example demonstrates the multiphase control of the thiosulfate ozonation reaction mechanism.

4. Conclusions

One of the key challenges when investigating multiphase chemistry is connecting molecular-level detail to macroscale reactivity in different phases. Here, we use DUV-SHG, which provides information about the first few layers of molecules at an aqueous surface, APXPS, which provides information from about the first ~1.5 to 5 nm at an aqueous surface, and reaction kinetics in trapped droplets, which provides information about reactivity across the interface and bulk. These three techniques, representing vastly different length scales, are combined using stochastic kinetic modeling *via* Kinetiscope©. The resultant kinetic model is used to explore the relationship between a complex reaction mechanism, the ozonation of thiosulfate, and the multiphase nature of the droplet reactor. Specifically, we find that individual reaction steps tend to occur throughout smaller droplets, where the reacto-diffusive length nears the droplet radius, while individual reaction steps become separated in larger droplets, where the reacto-diffusive length is much smaller than the droplet radius. Specifically, primary reaction steps typically occur more often at the interface than in the bulk, while some downstream reaction steps occur predominantly in the bulk. We also find that the product distribution, and thus the average sulfur oxidation state, is dependent on a non-trivial combination of droplet size and reactant concentration.

31

$S_2O_3^{2-}$ has two sulfurs with an average oxidation state of +2, while its ozonation products have a range of oxidation states. Fully oxidized sulfur (S^{+6}) in the form of sulfate attracts water, increasing the size of the aerosol/droplet or forming cloud condensation nuclei (CCN), directly affecting radiative forcing. While we show that most sulfate will be formed in the bulk of the droplet, in more acidic conditions some sulfate will be formed at the surface of the droplet, potentially increasing the likelihood that it can impact the surrounding environment. On the other hand, SO_2, $S_3O_6^{2-}$, and $S_4O_6^{2-}$ are incompletely oxidized with average sulfur oxidation states of +4, +3.3, and +2.5, respectively. The incompletely oxidized sulfur in these stable intermediates remains susceptible to further oxidation in large bodies of water or atmospheric aerosols/droplets, which typically also results in downstream acidification.

Recent efforts have suggested using ozone-microbubbles for mining wastewater remediation including thiosalt removal. This study shows that these processes should consider the size and pH of bubbles to ensure maximum sulfur oxidation and prevent downstream acidification of the natural environment. Additionally, the sulfur cycle, and specifically the oxidation state of sulfur, can have a large impact on the global radiation budget. Atmospheric chemistry models thus require a thorough understanding of sulfur chemistry to predict CCN formation and aerosol/droplet acidification. This study begins to address the relevant parameters for thorough modeling of potential thiosulfate ozonation occurring in the atmosphere. Similar studies addressing the multiphase chemistry in droplet reactors for other environmentally relevant reaction mechanisms can be used to obtain a more detailed understanding of atmospheric chemistry involving droplets and aerosols.

Data Availability

Data are available from the corresponding author upon request.

Author Contributions

Conceptualization: A.M.D and K.R.W. Kinetic modelling methodology: A.M.D, A.M.P, and K.R.W. Model implementation and simulations: A.M.D. DUV-SHG experimental methodology: F.B. and

32

R.J.S. DUV-SHG collection: F.B. APXPS experimental methodology: M.B. APXPS data collection: M.L.L., A.S., M.B. APXPS data analysis: A.S. Writing – original draft: A.M.D. Writing – review and editing: all.

Conflicts of Interest

There are no conflicts to declare.

Acknowledgements

References

1. Z. Wei, Y. Li, R. G. Cooks and X. Yan, Accelerated reaction kinetics in microdroplets: Overview and recent developments, *Ann. Rev. Phys. Chem*, 2020, **71**, 31-51.
2. G. Rovelli, M. I. Jacobs, M. D. Willis, R. J. Rapf, A. M. Prophet and K. R. Wilson, A critical analysis of electrospray techniques for the determination of accelerated rates and mechanisms of chemical reactions in droplets, *Chem. Sci.*, 2020, **11**, 13026-13043.
3. C. J. Chen and E. Williams, Are hydroxyl radicals spontaneously generated in unactivated water droplets?, *Angew. Chem.*, 2024, e202407433.
4. A. Gallo, A. S. Farinha, M. Dinis, A.-H. Emwas, A. Santana, R. J. Nielsen, W. A. Goddard and H. Mishra, The chemical reactions in electrosprays of water do not always correspond to those at the pristine air–water interface, *Chem. Sci.*, 2019, **10**, 2566-2577.
5. V. Masson-Delmotte, P. Zhai, A. Pirani, S. L. Connors, C. Péan, S. Berger, N. Caud, Y. Chen, L. Goldfarb and M. Gomis, IPC 2021. Summary for policymakers. Climate change 2021: The physical science Basis. Contribution of working group I to the sixth assessment report of the intergovernmental panel on climate change, 2023.
6. P. R. Veres, J. A. Neuman, T. H. Bertram, E. Assaf, G. M. Wolfe, C. J. Williamson, B. Weinzierl, S. Tilmes, C. R. Thompson and A. B. Thames, Global airborne sampling reveals a previously unobserved dimethyl sulfide oxidation mechanism in the marine atmosphere, *Proc. Natl. Acad. Sci.*, 2020, **117**, 4505-4510.
7. A. M. Deal, A. M. Prophet, F. Bernal, R. J. Saykally and K. R. Wilson, A detailed reaction mechanism for thiosulfate oxidation by ozone in aqueous environments, *Environ. Sci. Technol.*, 2024.
8. A. J. Atkinson, H. Ray and E. C. Wert, Efficiency of ozone quenching agents at different temperature, pH, and hydrodynamic conditions, *Ozone: Sci. Eng.*, 2024, 1-20.

9. S.-H. Hsu, F.-Y. Lin, G. G. Huang and Y.-P. Chang, Accelerated sulfur oxidation by ozone on surfaces of single optically trapped aerosol particles, *J. Phys. Chem. C*, 2023, **127**, 6248-6261.

10. A. M. Prophet, K. Polley, G. J. Van Berkel, D. T. Limmer and K. R. Wilson, Iodide oxidation by ozone at the surface of aqueous microdroplets, *Chem. Sci.*, 2024, **15**, 736-756.

11. M. D. Willis and K. R. Wilson, Coupled interfacial and bulk kinetics govern the timescales of multiphase ozonolysis reactions, *J. Phys. Chem. A*, 2022, **126**, 4991-5010.

12. M. Takizawa, A. Okuwaki and T. Okabe, The chemical behavior of low valence sulfur compounds. VIII. the oxidation of sodium thiosulfate with ozone, *Bull. Chem. Soc. Jpn.*, 1973, **46**, 3785-3789.

13. H. M. Eckenrode, S.-H. Jen, J. Han, A.-G. Yeh and H.-L. Dai, Adsorption of a cationic dye molecule on polystyrene microspheres in colloids: Effect of surface charge and composition probed by second harmonic generation, *J. Phys. Chem. B*, 2005, **109**, 4646-4653.

14. P. B. Petersen and R. J. Saykally, Probing the interfacial structure of aqueous electrolytes with femtosecond second harmonic generation spectroscopy, *J. Phys. Chem. B*, 2006, **110**, 14060-14073.

15. D. E. Otten, P. R. Shaffer, P. L. Geissler and R. J. Saykally, Elucidating the mechanism of selective ion adsorption to the liquid water surface, *Proc. Natl. Acad. Sci.*, 2012, **109**, 701-705.

16. F. Bernal, A. Dodin, C. Kyprianou, D. T. Limmer and R. J. Saykally, Adsorption of guanidinium cations to the air-water interface, *arXiv preprint arXiv:2408.15423*, 2024.

17. M. J. Blandamer and M. F. Fox, Theory and applications of charge-transfer-to-solvent spectra, *Chem. Rev.*, 1970, **70**, 59-93.

18. M. I. Jacobs, J. F. Davies, L. Lee, R. D. Davis, F. Houle and K. R. Wilson, Exploring chemistry in microcompartments using guided droplet collisions in a branched quadrupole trap coupled to a single droplet, paper spray mass spectrometer, *Anal. Chem.*, 2017, **89**, 12511-12519.

19. M. D. Willis, G. Rovelli and K. R. Wilson, Combining mass spectrometry of picoliter samples with a multicompartment electrodynamic trap for probing the chemistry of droplet arrays, *Anal. Chem.*, 2020, **92**, 11943-11952.

20. A. Wiegel, K. Wilson, W. Hinsberg and F. Houle, Stochastic methods for aerosol chemistry: a compact molecular description of functionalization and fragmentation in the heterogeneous oxidation of squalane aerosol by OH radicals, *Phys. Chem. Chem. Phys.*, 2015, **17**, 4398-4411.

21. I. Langmuir, The adsorption of gases on plane surfaces of glass, mica and platinum, *J. Am. Chem. Soc.*, 1918, **40**, 1361-1403.

22. J. Vieceli, M. Roeselova, N. Potter, L. X. Dang, B. C. Garrett and D. J. Tobias, Molecular dynamics simulations of atmospheric oxidants at the air− water interface: solvation and accommodation of OH and O3, *J. Phys. Chem. B*, 2005, **109**, 15876-15892.

23. R. Sander, Compilation of Henry's law constants (version 5.0. 0) for water as solvent, *Atmos. Chem. Phys.*, 2023, **23**, 10901-12440.

24. N. Panich, B. Ershov, A. Seliverstov and A. Basiev, Ozone solubility in concentrated aqueous solutions of salts, *Russ. J. Appl. Chem.*, 2007, **80**, 1812-1815.

25. S. Gopalakrishnan, P. Jungwirth, D. J. Tobias and H. C. Allen, Air− liquid interfaces of aqueous solutions containing ammonium and sulfate: Spectroscopic and molecular dynamics studies, *J. Phys. Chem. B*, 2005, **109**, 8861-8872.

26. W. S. Drisdell, R. J. Saykally and R. C. Cohen, On the evaporation of ammonium sulfate solution, *Proc. Natl. Acad. Sci.*, 2009, **106**, 18897-18901.

34

27. Y. Litman, K.-Y. Chiang, T. Seki, Y. Nagata and M. Bonn, Surface stratification determines the interfacial water structure of simple electrolyte solutions, *Nat. Chem.*, 2024, **16**, 644-650.

28. L. M. Pegram and M. T. Record, Hofmeister salt effects on surface tension arise from partitioning of anions and cations between bulk water and the air− water interface, *J. Phys. Chem. B*, 2007, **111**, 5411-5417.

29. T. Seki, C.-C. Yu, K.-Y. Chiang, A. Greco, X. Yu, F. Matsumura, M. Bonn and Y. Nagata, Ions speciation at the water–air interface, *J. Am. Chem. Soc.*, 2023, **145**, 10622-10630.

30. H.-t. Bian, R.-r. Feng, Y.-y. Xu, Y. Guo and H.-f. Wang, Increased interfacial thickness of the NaF, NaCl and NaBr salt aqueous solutions probed with non-resonant surface second harmonic generation (SHG), *Phys. Chem. Chem. Phys.*, 2008, **10**, 4920-4931.

31. S. W. Devlin, S. Jamnuch, Q. Xu, A. A. Chen, J. Qian, T. A. Pascal and R. J. Saykally, Agglomeration drives the reversed fractionation of aqueous carbonate and bicarbonate at the air–water interface, *J. Am. Chem. Soc.*, 2023, **145**, 22384-22393.

32. L. Onsager and N. N. Samaras, The surface tension of Debye-Hückel electrolytes, *J. Chem. Phys.*, 1934, **2**, 528-536.

33. R. K. Lam, J. W. Smith, A. M. Rizzuto, O. Karslıoğlu, H. Bluhm and R. J. Saykally, Reversed interfacial fractionation of carbonate and bicarbonate evidenced by X-ray photoemission spectroscopy, *J. Chem. Phys.*, 2017, **146**.

34. Z. Tao, J. Goodisman and A.-K. Souid, Oxygen measurement via phosphorescence: reaction of sodium dithionite with dissolved oxygen, *J. Phys. Chem. A*, 2008, **112**, 1511-1518.

35. G. Merényi, J. Lind, S. Naumov and C. von Sonntag, The reaction of ozone with the hydroxide ion: mechanistic considerations based on thermokinetic and quantum chemical calculations and the role of HO_4^- in superoxide dismutation, *Chem. Eur. J.*, 2010, **16**, 1372-1377.

36. J. R. Kanofsky and P. D. Sima, Reactive absorption of ozone by aqueous biomolecule solutions: implications for the role of sulfhydryl compounds as targets for ozone, *Arch. Biochem. Biophys.*, 1995, **316**, 52-62.

37. B. Müller and M. R. Heal, The mass accommodation coefficient of ozone on an aqueous surface, *Phys. Chem. Chem. Phys.*, 2002, **4**, 3365-3369.

38. H. O. Pye, A. Nenes, B. Alexander, A. P. Ault, M. C. Barth, S. L. Clegg, J. L. Collett Jr, K. M. Fahey, C. J. Hennigan and H. Herrmann, The acidity of atmospheric particles and clouds, *Atmos. Chem. Phys.*, 2020, **20**, 4809-4888.

39. B. J. Finlayson-Pitts and J. N. Pitts Jr, Particles in the troposphere, in *Chemistry of the upper and lower atmosphere: theory, experiments, and applications*, Elsevier, 1999.